Figure 3. Network generation using Ingenuity Pathway Analysis. The "Increased Levels of Albumin, Amino Acid Metabolism, Molecular Transport" network was associated with metabolites that were significantly different between JHH7 and Hc cells (*A*) and the metabolites that were differentially regulated by ACR in JHH7 cells (*B*). Up-regulated metabolites are indicated in red, down-regulated metabolites indicated in green, and metabolites that were not annotated in this study but are part of this network are indicated in white. Direct relationships are drawn with solid arrows, and indirect relationships are drawn with dashed arrows.
doi:10.1371/journal.pone.0082860.g003

Statistical and multivariate analyses

All the experiments in this study were performed independently two or more times to ensure the reproducibility of the results. Quantitative data were expressed as the means ± SEMs. The statistical significance of differences between values was assessed using a two-tailed Student's *t*-test or a Mann-Whitney U test. Values of $P<0.05$ were considered to indicate statistical significance. Unsupervised principal component analysis (PCA) was run using SIMCA-P+ software (Version 12.0, Umetrics, Umeå, Sweden).

Results

The effect of ACR on the metabolism of JHH7 cells detected using ^{1}H-NMR

First, NMR-based metabolomics was performed to investigate the effect of ACR treatment on the metabolism of JHH7 cells. As shown in Figure S1, PCA analysis of the NMR spectra indicated that treatment with ACR for 4 h had a very minor effect on the metabolism of JHH7 cells, while obvious changes were observed after 18 h of ACR treatment compared to the EtOH control.

Differences between the metabolic profiles of JHH7 and Hc cells treated with EtOH and ACR detected using CE-TOFMS

To further investigate the cancer-selective effect of ACR, the metabolic profiles of JHH7 and Hc cells treated with EtOH and ACR for 24 h was measured using CE-TOFMS analysis. A total of 229 peaks (109 cationic and 120 anionic) were detected in either JHH7 or Hc cells; from these 229 peaks, 88 principal metabolites were quantified (Table S2). The metabolic pathways of all the detected metabolites are illustrated in Figure 1. These metabolites are associated with glycolysis/gluconegenesis, the pentose phosphate pathway, the tricarboxylic acid cycle, the urea cycle, pyrimidine metabolism, nicotinate and nicotinamide metabolism and amino acid metabolism. The result of the comparison of the metabolic profiles of the cells is provided in Figure 2. PCA analysis revealed a very clear distinction between the abundance of intracellular metabolites of JHH7 and Hc cells with and without ACR treatment (Figure 2A), while the first component (PC1) indicated that 67% of the total variance is due to the difference between JHH7 and Hc cells. PC2 (11.2%) indicated that the ACR-treated JHH7 cells have a metabolic profile that is similar to that of the EtOH-treated Hc cells. Furthermore, heatmap analysis indicated that the metabolic pattern of JHH7 cells was almost completely opposite that of the Hc cells; a similar difference was observed between the ACR-treated and EtOH-treated JHH7 cells (Figure 2B). Finally, the cellular content of 71 metabolites in JHH7 and Hc cells was significantly different with *P* values less than 0.05 and fold changes greater than 1.2; 58 metabolites were significantly down-regulated by ACR in JHH7 cells compared to the EtOH control. Forty-nine common metabolites were shared between the two groups (Figure 2C).

Network generation and pathway analyses

Next, the list of the significantly different metabolites was imported into the IPA platform to investigate possible biological interactions. The biological functions of the top five IPA-generated networks and top five canonical metabolic pathways are summarized in Tables 1 and 2, respectively, and shown in Figure 3. Interestingly, IPA analysis indicated that the most highly populated biological network ("Increased Levels of Albumin, Amino Acid Metabolism, Molecular Transport") and the top two canonical metabolic pathways ("tRNA Charging" and "Purine Nucleotides De Novo Biosynthesis II") that were associated with the ACR-regulated metabolites by in JHH7 cells were the same as the networks that were associated with metabolic differences between JHH7 and Hc cells.

Table 1. Top five associated network functions generated by IPA.

	Top function	Score
EtOH-treated JHH7 vs. Hc	Increased Levels of Albumin, Amino Acid Metabolism, Molecular Transport	39
	Cellular Growth and Proliferation, Organismal Development, Cellular Compromise	21
	Cardiovascular System Development and Function, Organ Development, Carbohydrate Metabolism	18
	Cellular Growth and Proliferation, Organismal Development, Small Molecule Biochemistry	16
	Carbohydrate Metabolism, Cell Morphology, Cell-To-Cell Signaling and Interaction	11
ACR vs. EtOH-treated JHH7	Increased Levels of Albumin, Amino Acid Metabolism, Molecular Transport	38
	Carbohydrate Metabolism, Molecular Transport, Small Molecule Biochemistry	23
	Cellular Growth and Proliferation, Organismal Development, Small Molecule Biochemistry	16
	Free Radical Scavenging, Small Molecule Biochemistry, Molecular Transport	14
	Post-Translational Modification, Cellular Assembly and Organization, Developmental Disorder	6

doi:10.1371/journal.pone.0082860.t001

Table 2. Top canonical pathways identified by IPA.

	Top canonical pathway	P-Value
EtOH-treated JHH7 vs. Hc	tRNA Charging	6.82E-30
	Purine Nucleotides De Novo Biosynthesis II	1.30E-24
	Pyrimidine Ribonucleotides De Novo Biosynthesis	9.94E-20
	Superpathway of Citrulline Metabolism	9.93E-19
	Gluconeogenesis I	8.21E-18
ACR vs. EtOH-treated JHH7	tRNA Charging	9.48E-30
	Purine Nucleotides De Novo Biosynthesis II	2.91E-19
	Arginine Biosynthesis IV	3.10E-15
	Citrulline-Nitric Oxide Cycle	1.84E-14
	NAD biosynthesis II (from tryptophan)	5.72E-14

doi:10.1371/journal.pone.0082860.t002

ACR inhibits the increase in adenosine-5′-triphosphate (ATP) production in JHH7 cells

A comparison of the biosynthetic metabolites (nucleotides, amino acids and lipids) in the EtOH- or ACR-treated JHH7 and Hc cells determined by CE-TOFMS is summarized in Table 3. Of particular interest, the changes in the concentrations of adenosine nucleotides are shown in Figure 4. Notably, ATP levels were 1.6-fold higher in the EtOH-treated JHH7 cells than in the EtOH-treated Hc cells; ACR suppressed this increase, nearly to the basal levels observed in Hc cells (0.72-fold and $P = 0.00015$ compared to the EtOH-treated JHH7 cells). In contrast, only a very minor effect of ACR was observed on the levels of adenosine diphosphate (ADP) and adenosine monophosphate (AMP) in JHH7 cells (0.84- and 0.82-fold compared to the EtOH control, respectively).

ACR enhances PDK4 expression in JHH7 cells, but not in Hc cells

To further understand the cancer-selective inhibitory effect of ACR on ATP production, a set of genes that is known to be important in the regulation of energy metabolism in cancer cells was selected based on previous reports [26,27,28,29], and the effect of ACR on the expression of these genes was measured using real-time PCR (Figure 5A). Of particular interest, we found that ACR significantly enhanced the expression of PDK4, an important regulator of ATP levels [30], in JHH7 cells but not in Hc cells (3.06-fold; $P = 0.0033$ and 1.20-fold; $P = 0.062$, respectively; Figure 5B). Further western blot analysis revealed a nearly 2-fold increase in PDK4 protein levels after ACR treatment, but ACR did not affect the phosphorylation of PDHA1 in JHH7 cells (Figure 5C).

Functional analysis of PDK4 in JHH7 cells

Furthermore, loss-of-function experiments were performed to confirm the role of PDK4 in the effect of ACR on cellular ATP levels and the proliferation of JHH7 cells. As shown in Figure 6A, treatment with an siRNA targeting PDK4 (siPDK4) caused a dose-dependent downregulation of PDK4 mRNA expression (0.57-fold and 0.41-fold compared to siControl-treated cells with 50 nM and 100 nM siPDK4, respectively). Interestingly, ACR weakly but significantly inhibited cellular ATP levels in siControl-treated JHH7 cells (0.88-fold and $P = 0.042$ compared with EtOH). In contrast, no significant effect was observed in siPDK4-treated JHH7 cells (1.07-fold and $P = 0.42$ compared with EtOH; Figure 6B). However, PDK4 knockdown did not rescue the inhibitory effect of ACR on the proliferation of JHH7 cells (Figure 6C).

Clinical expression levels of PDK4

The mining of microarray data from a human HCC data set revealed that PDK4 mRNA is significantly down-regulated in liver tumors compared to adjacent non-tumor liver tissues (0.66-fold, $P = 3.11E\text{-}85$; Figure 7A). Finally, a PDK4-dependent regulatory network that involves RXR and peroxisome proliferator-activated

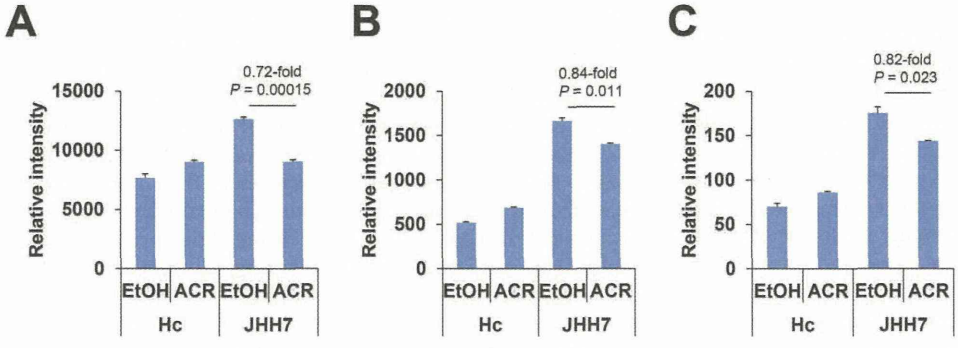

Figure 4. Levels of adenosine nucleotides in EtOH or ACR-treated JHH7 and Hc cells determined by CE-TOFMS. ATP (*A*), ADP (*B*) and AMP (*C*) levels.
doi:10.1371/journal.pone.0082860.g004

Table 3. Comparison of biosynthetic metabolites in EtOH or ACR-treated JHH7 and Hc cells determined by CE-TOFMS.

Biosynthetic pathways	Metabolites	KEGG	Fold change			
			EtOH-treated JHH7 vs. Hc		ACR vs. EtOH-treated JHH7	
			Mean	SEM	Mean	SEM
Nucleotide biosynthesis	AMP	C00020	2.50	0.10	0.82	0.00
	ATP	C00002	1.64	0.02	0.72	0.01
	CTP	C00063	1.84	0.11	0.74	0.05
	dATP	C00131	1.26	0.02	0.47	0.07
	dCTP	C00458	2.74	0.06	0.69	0.07
	dTTP	C00459	1.96	0.04	0.61	0.06
	GDP	C00035	2.76	0.15	0.82	0.02
	GTP	C00044	1.67	0.11	0.74	0.04
	IMP	C00130	2.33	0.11	0.71	0.08
	PRPP	C00119	0.68	0.08	0.53	0.11
	Ribulose 5-P	C00199	0.46	0.05	0.68	0.05
	UDP	C00015	2.81	0.05	0.82	0.05
	UTP	C00075	1.22	0.04	0.68	0.02
Amino acid biosynthesis	Ala	C00041	9.23	0.31	0.79	0.02
	Asp	C00049	3.23	0.08	0.77	0.01
	Glu	C00025	1.38	0.02	0.76	0.01
	Gly	C00037	0.64	0.02	0.82	0.01
	Ile	C00407	0.80	0.03	0.79	0.01
	Leu	C00123	0.73	0.03	0.78	0.02
	Lys	C00047	1.94	0.06	0.77	0.03
	Phe	C00079	0.69	0.02	0.78	0.01
	Ser	C00065	5.31	0.20	0.81	0.02
	Thr	C00188	1.94	0.07	0.77	0.00
	Trp	C00078	0.06	0.00	0.78	0.02
	Tyr	C00082	0.71	0.03	0.79	0.02
	Val	C00183	0.83	0.04	0.78	0.02
Lipid biosynthesis	3-Hydroxybutyric acid	C01089	1.58	0.03	0.82	0.03
	DHAP	C00111	0.28	0.03	0.52	0.03

doi:10.1371/journal.pone.0082860.t003

receptors (PPARs) and summarizes the effects of ACR on ATP production was generated using IPA (Figure 7B).

Discussion

The war on cancer has continued for more than 40 years, but the gains have been limited. One potential reason for this limited success that typical drug development in oncology has focused on targets that are essential for the survival of all dividing cells, leading to narrow therapeutic windows [31]. Recent advances in metabolite profiling methodologies have generated an alternative window for cancer therapy in targeting cancer metabolism [13]. ACR, a very promising drug that is currently in clinical trials for HCC treatment, has been shown to markedly prevent the recurrence of HCC [3] and selectively inhibit HCC cell growth [5]. We have previously exploited the potential target molecules of ACR that are associated with the promotion of tumor cell proliferation [5] or angiogenesis [32]. In this study, we performed metabolome analyses in JHH7 and Hc cells treated with ACR using both NMR and CE-TOFMS technologies to further understand the molecular pathways that underlie the cancer-selective growth suppressive effect of ACR. We found that ACR selectively suppressed the enhanced nucleotide synthesis and energy metabolism of HCC cells, suggesting that metabolic pathways may be important targets for ACR's anti-cancer activity. The further study of these pathways will benefit the development of more effective cancer drugs and therapies against HCC.

Generally, the metabolic patterns of JHH7 and Hc cells were almost completely opposite to each other (Figure 2), which is consistent with previous reports that cancer cells exhibit considerably different metabolic requirements than most normal differentiated cells and supports the hypothesis that cancer may be a type of metabolic disease [33]. Although the primary cause of cancer is assumed to be at the level of gene expression, metabolites can be considered to be the end products of the cellular regulatory processes that underlie malignant cell growth such as genome instability and mutability [34]. Metabolomic comparison of HCC and control liver tissues have been carried out in several animal and human studies aiming to define metabolomic biomarkers for the early detection of HCC [35,36]. In this study, the abundance

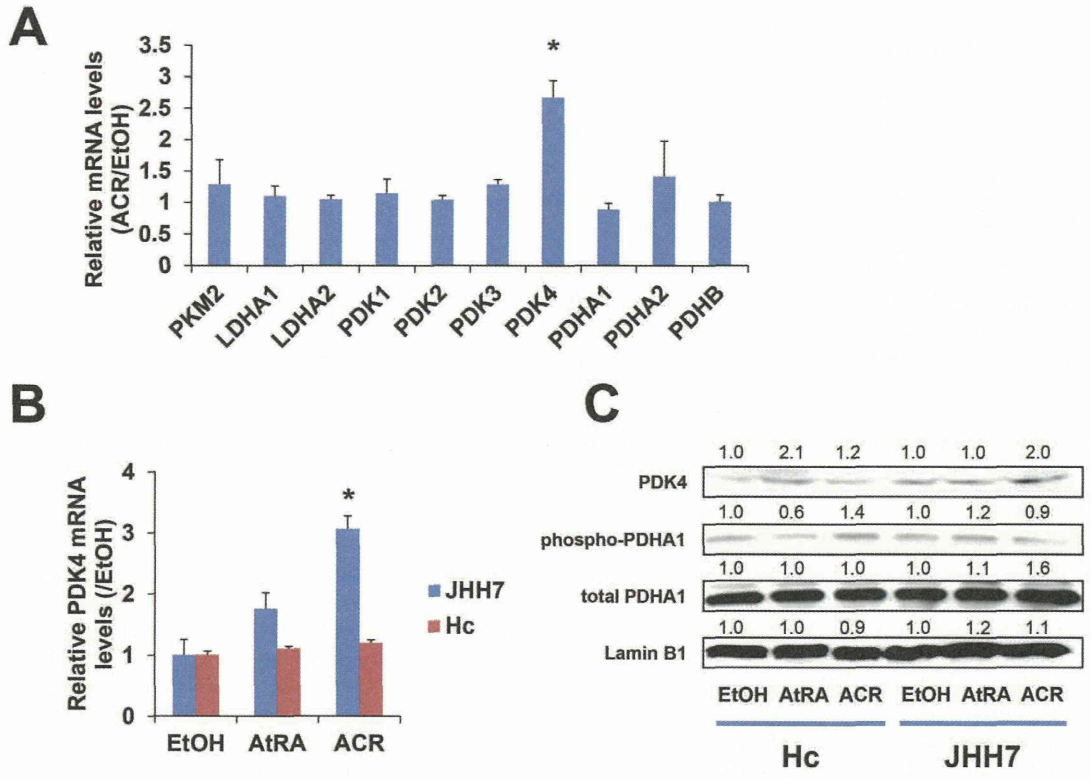

Figure 5. ACR increase the expression of PDK4 in JHH7 cells but not Hc cells. The effect of ACR on the expression of genes related to energy metabolism and ATP production in cancer cells (*A*). Levels of PDK4 mRNA (*B*) and levels of PDH4, phospho-PDHA1 and total PDHA1 protein (*C*) in JHH7 and Hc cells treated with EtOH, AtRA and ACR. The statistical significance of difference was evaluated using the Student's *t*-test.
doi:10.1371/journal.pone.0082860.g005

of 71 metabolites was found to be significantly different between JHH7 and Hc cells; 49 of these metabolites were significantly down-regulated by ACR in JHH7 cells (Figure 2 and Table S2). It is not unexpected that an IPA analysis revealed that most of these metabolites are involved in the amino acids and nucleotide biosynthetic pathways, such as "tRNA Charging", "Purine Nucleotides De Novo Biosynthesis II" and "Pyrimidine Ribonucleotides De Novo Biosynthesis" (Tables 2 and 3). It is well known that cancer cell metabolism must provide a large increase in lipid, protein, and nucleotide synthesis (biomass) to support their uncontrolled high rate of cell growth and proliferation [13]. Our findings indicate that ACR may exert its anti-cancer effect by blocking the biosynthetic processes of cancer cells. Interestingly, a bioinformatics-based anticancer drug screening program in Japan revealed that ACR shares similar anticancer activity pattern with the antipyrimidine drugs doxifluridine and cytarabine and an antipurine drug, 6-mercaptopurine, as assayed by growth inhibition against a panel of 39 human cancer cell lines (JFC39) [37,38,39].

ATP is the main energy source for the majority of cellular functions, and impaired cellular energy metabolism is the defining characteristic of nearly all cancers regardless of cellular or tissue

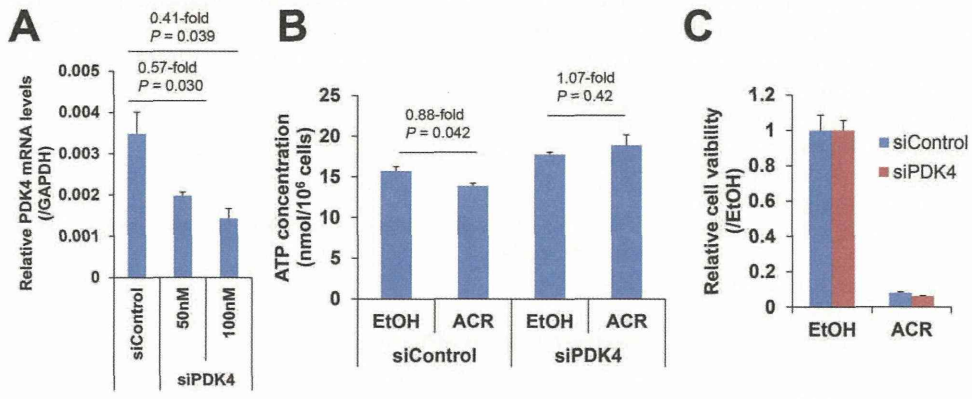

Figure 6. Functional analysis of PDK4 in JHH7 cells. The effect of siPDK4 on PDK4 gene expression (*A*). The effect of 50 nM siPDK4 on the ACR-mediated cellular ATP levels (*B*) and the proliferation (*C*) of JHH7 cells.
doi:10.1371/journal.pone.0082860.g006

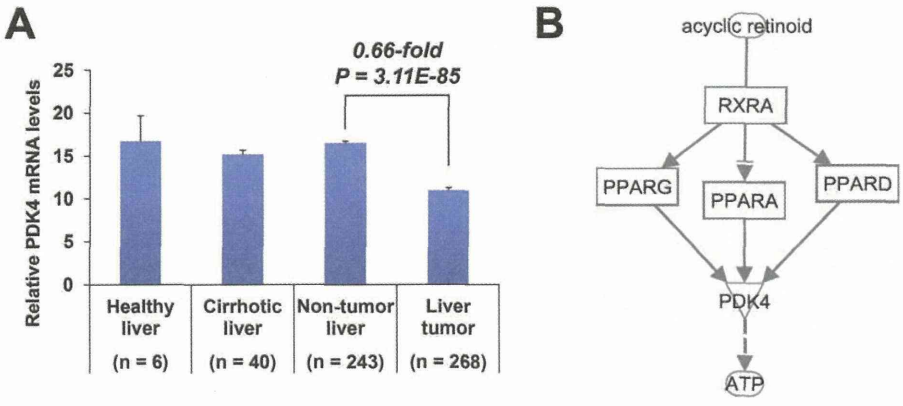

Figure 7. Clinical expression levels of PDK4. The expression of PDK4 mRNA in human liver cancer (GEO data set GSE25097) (*A*). Statistical significance was evaluated using the Mann-Whitney U test. A schematic model of the PDK4-denpendent regulatory network of ACR on ATP production in JHH7 cells generated using IPA (*B*).
doi:10.1371/journal.pone.0082860.g007

origin [33]. Of particular interest, ACR can selectively inhibit the production of ATP in JHH7 cells but not in Hc cells (Figure 4). It has been proven that chemical depletion of ATP can inhibit the growth of HCC cells [40]. This may partially explain the cancer-selective growth suppression effect of ACR. To further understand the molecular signaling mechanisms that underlie this effect, we examined the effect of ACR on the expression of energy production-related genes and observed that the expression of PDK4 was significantly enhanced by ACR in JHH7 cells but not in Hc cells (Figure 5). PDK4 is a key regulator of tricarboxylic acid (TCA) cycle; PDK4 phosphorylates and inactivates the pyruvate dehydrogenase (PDH) complex and thereby switches the energy source for the production of ATP from glucose to fatty acids. Although the cellular pyruvate level was not detected by CE-TOFMS and no effect of ACR was found on the phosphorylation of PDHA1 by western blot analysis (Figure 5C), the knockdown of PDK4 expression using RNA interference in JHH7 cells can rescue the decreased cellular ATP levels induced by ACR (Figure 6B), suggesting that PDK4 may be an important feature of ACR's anti-cancer activity. Moreover, we performed data mining using the GEO database and found that PDK4 expression is significantly down-regulated in liver tumors compared to adjacent non-tumor liver tissues (Figure 7A). The role of PDK4 in cancer therapy is complex; the inhibition of PDK4 is sufficient to inhibit the proliferation of and induce apoptosis in lung cancer cells [41], but the overexpression of PDK4 is also able to decrease ATP levels and suppress de novo lipogenesis and proliferation in breast cancer cells [30]. The specific role of PDK4 in HCC remains to be fully determined. Our results suggest that PDK4 up-regulation has a suppressive effect on HCC. Consistent with this implication, the results of IPA analysis suggest that the cancer-selective, growth-suppressive effect of ACR in inhibiting the ATP production of HCC cells may be related to a putative PDK4-dependent molecular signaling mechanism involving RXR and PPARs, as has been reported in certain fatty acid signaling pathways [42] (Figure 7B).

Although the Warburg effect is a well-recognized hallmark of cancer metabolism, it remains controversial [43]. Warburg hypothesized that tumor cells convert most of their glucose to lactate due to mitochondrial defects. However, subsequent studies showed that most tumor mitochondria are not defective in their ability to carry out oxidative phosphorylation [43]. In fact, we propose that mitochondrial oxidative phosphorylation may be important in supporting HCC cell proliferation based on the following observations: 1) the content of lactate, the major end product of glycolysis, is lower in JHH7 cells than in Hc cells (0.40-fold, Table S2) and 2) ACR up-regulates the expression of PDK4, which attenuates the flux of glycolytic carbon into mitochondrial oxidation and can reduce the production of ATP and inhibit the growth of JHH7 cells.

In summary, our study is the first to investigate the effect of ACR on cancer cell metabolism. A comparison of the metabolic effects of ACR in JHH7 and Hc cells was performed, and a JHH7-selective inhibitory effect of ACR on the production of ATP was observed. The underlying molecular signaling mechanism may relate in part to the cancer-selective enhancement of PDK4 expression, suggesting that mitochondrial oxidative phosphorylation is important in the energy metabolism of HCC cells. However, it should be noted that although PDK4 knockdown can rescue the decreased cellular ATP levels induced by ACR, no effect was observed on the inhibitory effect of ACR on the proliferation of JHH7 cells. Further research is needed to combine the cancer-selective metabolic pathways identified in this study and other signaling pathways to increase our knowledge of ACR's selective anti-cancer activity and to develop more effective cancer drugs and therapies to help us win the war against HCC.

Supporting Information

Figure S1 Statistical analysis of metabolites in JHH7 cells detected by ^{1}H-NMR. PCA score plots of the NMR spectra of JHH7 cells treated with EtOH or 10 μM ACR for 4 h and 18 h (*A*) or only 18 h (*B*).
(PPTX)

Table S1 The primers used in this study.
(XLSX)

Table S2 Quantification of major metabolites in JHH7 and Hc cells.
(XLSX)

Author Contributions

Conceived and designed the experiments: XYQ MT MS HM SK. Performed the experiments: XYQ FW. Analyzed the data: XYQ. Contributed reagents/materials/analysis tools: NI. Wrote the paper: XYQ SK.

References

1. Venook AP, Papandreou C, Furuse J, de Guevara LL (2010) The incidence and epidemiology of hepatocellular carcinoma: a global and regional perspective. Oncologist 15 Suppl 4: 5–13.
2. Llovet JM, Schwartz M, Mazzaferro V (2005) Resection and liver transplantation for hepatocellular carcinoma. Semin Liver Dis 25: 181–200.
3. Muto Y, Moriwaki H, Ninomiya M, Adachi S, Saito A, et al. (1996) Prevention of second primary tumors by an acyclic retinoid, polyprenoic acid, in patients with hepatocellular carcinoma. Hepatoma Prevention Study Group. N Engl J Med 334: 1561–1567.
4. Muto Y, Moriwaki H, Saito A (1999) Prevention of second primary tumors by an acyclic retinoid in patients with hepatocellular carcinoma. N Engl J Med 340: 1046–1047.
5. Tatsukawa H, Sano T, Fukaya Y, Ishibashi N, Watanabe M, et al. (2011) Dual induction of caspase 3- and transglutaminase-dependent apoptosis by acyclic retinoid in hepatocellular carcinoma cells. Mol Cancer 10: 4.
6. Obora A, Shiratori Y, Okuno M, Adachi S, Takano Y, et al. (2002) Synergistic induction of apoptosis by acyclic retinoid and interferon-beta in human hepatocellular carcinoma cells. Hepatology 36: 1115–1124.
7. Okada H, Honda M, Campbell JS, Sakai Y, Yamashita T, et al. (2012) Acyclic retinoid targets platelet-derived growth factor signaling in the prevention of hepatic fibrosis and hepatocellular carcinoma development. Cancer Res 72: 4459–4471.
8. Shao RX, Otsuka M, Kato N, Taniguchi H, Hoshida Y, et al. (2005) Acyclic retinoid inhibits human hepatoma cell growth by suppressing fibroblast growth factor-mediated signaling pathways. Gastroenterology 128: 86–95.
9. Kagawa M, Sano T, Ishibashi N, Hashimoto M, Okuno M, et al. (2004) An acyclic retinoid, NIK-333, inhibits N-diethylnitrosamine-induced rat hepatocarcinogenesis through suppression of TGF-alpha expression and cell proliferation. Carcinogenesis 25: 979–985.
10. Matsushima-Nishiwaki R, Okuno M, Takano Y, Kojima S, Friedman SL, et al. (2003) Molecular mechanism for growth suppression of human hepatocellular carcinoma cells by acyclic retinoid. Carcinogenesis 24: 1353–1359.
11. Suzui M, Masuda M, Lim JT, Albanese C, Pestell RG, et al. (2002) Growth inhibition of human hepatoma cells by acyclic retinoid is associated with induction of p21(CIP1) and inhibition of expression of cyclin D1. Cancer Res 62: 3997–4006.
12. Matsushima-Nishiwaki R, Okuno M, Adachi S, Sano T, Akita K, et al. (2001) Phosphorylation of retinoid X receptor alpha at serine 260 impairs its metabolism and function in human hepatocellular carcinoma. Cancer Res 61: 7675–7682.
13. Vander Heiden MG (2011) Targeting cancer metabolism: a therapeutic window opens. Nat Rev Drug Discov 10: 671–684.
14. Koppenol WH, Bounds PL, Dang CV (2011) Otto Warburg's contributions to current concepts of cancer metabolism. Nat Rev Cancer 11: 325–337.
15. Butler EB, Zhao Y, Munoz-Pinedo C, Lu J, Tan M (2013) Stalling the engine of resistance: targeting cancer metabolism to overcome therapeutic resistance. Cancer Res 73: 2709–2717.
16. El-Serag HB (2012) Epidemiology of viral hepatitis and hepatocellular carcinoma. Gastroenterology 142: 1264–1273 e1261.
17. Welzel TM, Graubard BI, Zeuzem S, El-Serag HB, Davila JA, et al. (2011) Metabolic syndrome increases the risk of primary liver cancer in the United States: a study in the SEER-Medicare database. Hepatology 54: 463–471.
18. Fujise K, Nagamori S, Hasumura S, Homma S, Sujino H, et al. (1990) Integration of hepatitis B virus DNA into cells of six established human hepatocellular carcinoma cell lines. Hepatogastroenterology 37: 457–460.
19. Qin XY, Wei F, Yoshinaga J, Yonemoto J, Tanokura M, et al. (2011) siRNA-mediated knockdown of aryl hydrocarbon receptor nuclear translocator 2 affects hypoxia-inducible factor-1 regulatory signaling and metabolism in human breast cancer cells. FEBS Lett 585: 3310–3315.
20. Wei F, Furihata K, Hu F, Miyakawa T, Tanokura M (2010) Complex mixture analysis of organic compounds in green coffee bean extract by two-dimensional NMR spectroscopy. Magn Reson Chem 48: 857–865.
21. Ohashi Y, Hirayama A, Ishikawa T, Nakamura S, Shimizu K, et al. (2008) Depiction of metabolome changes in histidine-starved Escherichia coli by CE-TOFMS. Mol Biosyst 4: 135–147.
22. Sugimoto M, Hirayama A, Robert M, Abe S, Soga T, et al. (2010) Prediction of metabolite identity from accurate mass, migration time prediction and isotopic pattern information in CE-TOFMS data. Electrophoresis 31: 2311–2318.
23. Qin XY, Akanuma H, Wei F, Nagano R, Zeng Q, et al. (2012) Effect of low-dose thalidomide on dopaminergic neuronal differentiation of human neural progenitor cells: a combined study of metabolomics and morphological analysis. Neurotoxicology 33: 1375–1380.
24. Qin XY, Kojima Y, Mizuno K, Ueoka K, Muroya K, et al. (2012) Identification of novel low-dose bisphenol a targets in human foreskin fibroblast cells derived from hypospadias patients. PLoS One 7: e36711.
25. Bronner IF, Bochdanovits Z, Rizzu P, Kamphorst W, Ravid R, et al. (2009) Comprehensive mRNA expression profiling distinguishes tauopathies and identifies shared molecular pathways. PLoS One 4: e6826.
26. Vander Heiden MG, Lunt SY, Dayton TL, Fiske BP, Israelsen WJ, et al. (2011) Metabolic pathway alterations that support cell proliferation. Cold Spring Harb Symp Quant Biol 76: 325–334.
27. Vander Heiden MG, Cantley LC, Thompson CB (2009) Understanding the Warburg effect: the metabolic requirements of cell proliferation. Science 324: 1029–1033.
28. Levine AJ, Puzio-Kuter AM (2010) The control of the metabolic switch in cancers by oncogenes and tumor suppressor genes. Science 330: 1340–1344.
29. DeBerardinis RJ, Lum JJ, Hatzivassiliou G, Thompson CB (2008) The biology of cancer: metabolic reprogramming fuels cell growth and proliferation. Cell Metab 7: 11–20.
30. Grassian AR, Metallo CM, Coloff JL, Stephanopoulos G, Brugge JS (2011) Erk regulation of pyruvate dehydrogenase flux through PDK4 modulates cell proliferation. Genes Dev 25: 1716–1733.
31. Michelakis ED, Webster L, Mackey JR (2008) Dichloroacetate (DCA) as a potential metabolic-targeting therapy for cancer. Br J Cancer 99: 989–994.
32. Komi Y, Sogabe Y, Ishibashi N, Sato Y, Moriwaki H, et al. (2010) Acyclic retinoid inhibits angiogenesis by suppressing the MAPK pathway. Lab Invest 90: 52–60.
33. Seyfried TN, Shelton LM (2010) Cancer as a metabolic disease. Nutr Metab (Lond) 7: 7.
34. Hanahan D, Weinberg RA (2011) Hallmarks of cancer: the next generation. Cell 144: 646–674.
35. Beyoglu D, Imbeaud S, Maurhofer O, Bioulac-Sage P, Zucman-Rossi J, et al. (2013) Tissue metabolomics of hepatocellular carcinoma: Tumor energy metabolism and the role of transcriptomic classification. Hepatology 58: 229–238.
36. Wang J, Zhang S, Li Z, Yang J, Huang C, et al. (2011) (1)H-NMR-based metabolomics of tumor tissue for the metabolic characterization of rat hepatocellular carcinoma formation and metastasis. Tumour Biol 32: 223–231.
37. Yamori T (2004) [Chemical evaluation by cancer cell line panel and its role in molecular target-based anticancer drug screening]. Gan To Kagaku Ryoho 31: 485–490.
38. (2004) Results of molecular target antineoplastic agents screening. Gan To Kagaku Ryoho 31 Suppl 1: 1–150.
39. Nakatsu N, Nakamura T, Yamazaki K, Sadahiro S, Makuuchi H, et al. (2007) Evaluation of action mechanisms of toxic chemicals using JFCR39, a panel of human cancer cell lines. Mol Pharmacol 72: 1171–1180.
40. Dilip A, Cheng G, Joseph J, Kunnimalaiyaan S, Kalyanaraman B, et al. (2013) Mitochondria-targeted antioxidant and glycolysis inhibition: synergistic therapy in hepatocellular carcinoma. Anticancer Drugs.
41. Bonnet S, Archer SL, Allalunis-Turner J, Haromy A, Beaulieu C, et al. (2007) A mitochondria-K+ channel axis is suppressed in cancer and its normalization promotes apoptosis and inhibits cancer growth. Cancer Cell 11: 37–51.
42. Schoonjans K, Staels B, Auwerx J (1996) Role of the peroxisome proliferator-activated receptor (PPAR) in mediating the effects of fibrates and fatty acids on gene expression. J Lipid Res 37: 907–925.
43. Ward PS, Thompson CB (2012) Metabolic reprogramming: a cancer hallmark even warburg did not anticipate. Cancer Cell 21: 297–308.

Biochemical and Biophysical Research Communications 443 (2014) 950–956

Contents lists available at ScienceDirect

Biochemical and Biophysical Research Communications

journal homepage: www.elsevier.com/locate/ybbrc

Neovessel formation promotes liver fibrosis via providing latent transforming growth factor-β

Kotaro Sakata [a,b,c], Satoshi Eda [a], Eun-Seo Lee [a], Mitsuko Hara [a], Masaya Imoto [b], Soichi Kojima [a,*]

[a] Micro-signaling Regulation Technology Unit, RIKEN Center for Life Science Technologies, Wako, Saitama 351-0198, Japan
[b] Department of Biosciences and Informatics, Faculty of Science and Technology, Keio University, Yokohama, Kanagawa 223-8522, Japan
[c] Drug Discovery Laboratory, Wakunaga Pharmaceutical Co., Ltd., Akitakata, Hiroshima 739-1195, Japan

ARTICLE INFO

Article history:
Received 10 December 2013
Available online 19 December 2013

Keywords:
Transforming growth factor-β
Liver fibrosis
Hepatic stellate cells
Liver sinusoidal endothelial cells

ABSTRACT

Aim: Hepatic fibrosis and angiogenesis occur in parallel during the progression of liver disease. Fibrosis promotes angiogenesis via inducing vascular endothelial growth factor (VEGF) from the activated hepatic stellate cells (HSCs). In turn, increased neovessel formation causes fibrosis, although the underlying molecular mechanism remains undetermined. In the current study, we aimed to address a role of endothelial cells (ECs) as a source of latent transforming growth factor (TGF)-β, the precursor of the most fibrogenic cytokine TGF-β.
Methods: After recombinant VEGF was administered to mice via the tail vein, hepatic angiogenesis and fibrogenesis were evaluated using immunohistochemical and biochemical analyses in addition to investigation of TGF-β activation using primary cultured HSCs and liver sinusoidal ECs (LSECs).
Results: In addition to increased hepatic levels of CD31 expression, VEGF-treated mice showed increased α-smooth muscle actin (α-SMA) expression, hepatic contents of hydroxyproline, and latency associated protein degradation products, which reflects cell surface activation of TGF-β via plasma kallikrein (PLK). Liberating the PLK-urokinase plasminogen activator receptor complex from the HSC surface by cleaving a tethering phosphatidylinositol linker with its specific phospholipase C inhibited the activating latent TGF-β present in LSEC conditioned medium and subsequent HSC activation.
Conclusion: Neovessel formation (angiogenesis) accelerates liver fibrosis at least in part via provision of latent TGF-β that activated on the surface of HSCs by PLK, thereby resultant active TGF-β stimulates the activation of HSCs.

1. Introduction

Liver fibrosis, a common feature of almost all chronic liver diseases, is caused by the excessive accumulation of extracellular matrix (ECM) proteins, including collagen produced mainly by hepatic stellate cells (HSCs) through the process termed activation [1–3]. Under physiological conditions, quiescent HSCs embrace sinusoids as liver-specific pericytes. When the liver parenchyma is chronically injured by various causes, HSCs detach from the sinusoids and subsequently transform into myofibroblast-like cells. This HSC activation is characterized by a loss of lipid droplets, the enhanced production of ECM, and the expression of activation markers such as α-smooth muscle actin (α-SMA) [4]. The HSC activation process is regulated by both autocrine and paracrine growth factors [4,5], among which transforming growth factor (TGF)-β, the most fibrogenic cytokine, plays a critical role [6,7].

TGF-β is produced as a high molecular weight latent form with its propeptide region known as "latency associated protein (LAP)", and thereby must be activated before exerting its biological activity [8]. Latent TGF-β is activated by plasma kallikrein (PLK), which is bound to glycophosphatidylinositol-anchored urokinase-type plasminogen activator receptor (uPAR) on the cell surface and released by phosphatidylinositol-specific phospholipase C (PI-PLC) [9]. PLK cleaves LAP between R58 and L59 during liver fibrosis [10]. After cleavage, the N-terminal side LAP degradation products ending at R58 (R58 LAP-DPs) remain within the ECM of the liver tissues through LTBP, serving as a footprint for active TGF-β generation. We produced a specific antibody (anti-R58 antibody) that detects a neoepitope at the cutting edge of R58 LAP-DPs [10].

Angiogenesis in the adult liver occurs both in pathological settings, such as cirrhosis and tumor development, and in physiological conditions such as liver regeneration [11,12]. Blood vessels in the liver are classified into the hepatic artery, portal vein and sinusoidal blood vessel groups. Thus, liver sinusoidal endothelial

* Corresponding author. Address: Micro-signaling Regulation Technology Unit, RIKEN Center for Life Science Technologies, 2-1 Hirosawa, Wako, Saitama 351-0198, Japan. Fax: +81 48 462 4675.
E-mail address: skojima@riken.jp (S. Kojima).

0006-291X/$ - see front matter © 2013 Elsevier Inc. All rights reserved.
http://dx.doi.org/10.1016/j.bbrc.2013.12.074

cells (LSECs) are the largest population of endothelial cells in the liver.

Hepatic angiogenesis and fibrogenesis occur in parallel during liver diseases [11,13]. Sahin et al. showed that VEGF transgenic mice with increased serum VEGF concentrations have augmented liver fibrosis [14]. However, how the overproduction of VEGF induces liver fibrosis has not yet been determined.

The current study addressed a role of ECs as a source of latent TGF-β, the precursor of the most fibrogenic cytokine TGF-β.

2. Materials and methods

2.1. Materials

Fluorescein isothiocyanate (FITC)-conjugated rat anti-mouse CD31 monoclonal antibody (Clone 390) and rat anti-mouse CD146 monoclonal antibody (Clone ME-9F1) were purchased from Millipore (Billerica, MA, USA) and Bio Legend (San Diego, CA, USA), respectively. FITC-conjugated mouse anti-α-SMA monoclonal antibody (Clone 1A4) and anti-α-SMA monoclonal antibody (Clone 1A4) were purchased from Sigma–Aldrich (St. Louis, MO, USA) and Dako (Glostrup, Denmark), respectively. Neutralizing mouse anti-TGF-β1 monoclonal antibody (Clone 9016) and sheep anti-rat IgG magnetic bead-conjugated antibody (Cat. No.110-35) were purchased from R&D Systems (Minneapolis, MN, USA) and Invitrogen (Carlsbad, CA, USA), respectively. Recombinant VEGF 165 and PI-PLC were purchased from Santa Cruz Biotechnology (Santa Cruz, CA, USA) and Sigma–Aldrich (St. Louis, MO, USA), respectively. An R58 monoclonal antibody that recognizes neo-epitopes formed via the PLK-dependent proteolytic activation of latent TGF-β1 was produced and characterized as previously reported [10].

2.2. Animal experiments

One hundred microliters of saline with or without recombinant VEGF 165 was injected intravenously via the tail veins of three 10-week-old C57BL/6 male mice (Japan SLC Inc., Shizuoka, Japan) daily at doses of 10 or 20 ng/g body weight for 10 days. The mice were euthanized, and the livers were harvested for biochemical and immunohistochemical analyses. All animal experiments were performed in compliance with the protocols approved by the RIKEN Institutional Animal Use and Care Administrative Advisory Committee.

2.3. Staining of liver tissue sections

Liver tissues were fixed in 4% paraformaldehyde (PFA) and embedded in paraffin, and tissue sections (6-μm thick) were prepared using a Leica sliding microtome (Leica Microsystems, Nussloch, Germany). The liver tissue sections were deparaffinized, rehydrated and incubated for 5 min with a drop of Proteinase K (Dako Envision) in 2 ml of 0.05 M Tris–HCl buffer (pH 7.5) at room temperature. Thereafter, endogenous peroxidase was blocked by incubation with 3% hydrogen peroxide in methanol at room temperature for 10 min. The liver tissue sections were stained with Myer's hematoxylin solution and 1% Eosin Y solution (Muto Pure Chemicals, Tokyo, Japan). For CD31 staining, liver sections were incubated at 4 °C overnight with rat anti-CD31 monoclonal antibody (5 μg/ml) and thereafter with the biotinylated rabbit anti-rat IgG antibody (1:200) included in the Vectastain Elite ABC kit for 30 min at room temperature. A 3,3′-diaminobenzidine (DAB) peroxidase substrate kit (Vector Laboratories, Inc., Burlingame, CA, USA) was used for its chromogenic substrate, which develops as a brown precipitate, to visualize immunolabeling. For α-SMA staining, liver sections were incubated at 4 °C overnight with mouse anti-α-SMA monoclonal antibody (1:100) and thereafter with DAKO Envision's polymer of antibodies labeled with peroxidase for 1 h at room temperature. The DAB peroxidase substrate kit was used for its chromogenic substrate. Sirius red, which results in the red staining of all fibrillary collagen, was used to evaluate fibrosis. The liver sections were stained with 0.05% Fast-green FCF (ChemBlink, Inc., CAS 2353-45-9) and 0.05% Direct red 80 (Polysciences, Inc., CAS 2610-10-18) in saturated picric acid (Muto Pure Chemicals) for 90 min at room temperature. Positive area analyses were performed using the WinROOF image analysis software from 3 randomly selected fields among 3 mice for a total of 9 samples per group.

2.4. Measurement of hepatic hydroxyproline content

The hepatic hydroxyproline content was measured as described by Reddy et al. [15]. Briefly, approximately 40 mg of frozen liver tissue was hydrolyzed in 2 N NaOH for 10 min at 65 °C, followed by incubation at 120 °C for 20 min. The same amount of 6 N HCl was added and incubated at 120 °C for 20 min. Activated charcoal solution (10 mg/ml in 4 N KOH) and 2.2 M acetic acid–0.48 M citric acid buffer (pH 6.5) were added to adjust the pH to 7–8. After centrifugation, 100 mM chloramine T solution was added to the supernatant and incubated at room temperature for 25 min. After the addition of 1 M Ehrlich's solution (*p*-dimethylaminobenzaldehyde), samples were incubated at 65 °C for 20 min. Absorbance was measured at 560 nm. The hydroxyproline content is expressed in μg/mg of sample protein.

2.5. Isolation of HSCs and LSECs

Primary HSCs were isolated from the livers of male C57BL/6 mice by collagenase/pronase digestion and the Nycodenz gradient method as described previously [9]; the cells were then cultured in Dulbecco's modified Eagle's medium (DMEM) containing 10% fetal bovine serum (FBS). Primary LSECs were isolated using a combination of rat anti-CD146 and sheep anti-rat IgG antibodies conjugated with magnetic beads from a fraction separated using the Nycodenz gradient method after the collagenase digestion of the livers of male C57BL/6 mice, according to the method described by Kitazume et al. [16]. The cells were then cultured in a DMEM/nutrient mixture F-12 (F12) containing 10% FBS.

2.6. Preparation of the LSEC conditioned medium (CM)

Briefly, 1×10^5 LSECs were seeded onto 6-well plates and precultured for 24 h with DMEM/F12 containing 10% FBS medium to grow the cells to confluency, followed by overnight starvation with DMEM/F12 containing 2% FBS at 37 °C. After the cells were rinsed with phosphate buffered saline (PBS), the medium was changed to 2 ml of DMEM/F12 containing 2% FBS and further cultured for 24 h to create LSEC CM.

2.7. Immunofluorescent staining

HSCs were fixed with 4% PFA for 10 min and incubated with 0.1% Triton X-100 in PBS for 20 min at room temperature. After blocking with 3% BSA in PBS for 40 min at room temperature, cells were incubated with FITC-conjugated anti-mouse α-SMA monoclonal antibody (1:200) for 2 h at room temperature. After being washed with PBS, the cells were mounted with Vectashield DAPI mounting medium (Vector Laboratories, Inc., Burlingame, CA, USA) and observed under a Zeiss LSM 700 laser scanning confocal microscope. The intensities of α-SMA and R58 LAP-DPs were calculated in each panel with ZEN software for quantitative fluorescence analyses.

2.8. Determination of the TGF-β concentration in CM

TGF-β was measured using a bioassay (luciferase assay in CCL64 cells) for active TGF-β and an enzyme-linked immunosorbent assay (ELISA) for total TGF-β. CCL64 cells, from the mink lung epithelial cell line, stably expressing $(CAGA)_9$-MLP-luciferase, which contains nine copies of an Smad binding CAGA box element upstream of a minimal adenovirus major late promoter [17], were plated at 2×10^4 cells/well in a 96-well plate with DMEM containing 10% FBS. On the next day, the medium was replaced with CM harvested from HSCs. After 6 h, the cells were extracted with a lysis buffer, and luciferase activity was measured using a Luciferase Assay System (Promega, Madison, WI, USA) according to the manufacturer's instructions. The amount of active TGF-β was calculated from a standard curve made with recombinant TGF-β1. The total TGF-β1 levels present in the LSEC CM before and after incubating with HSCs were determined using a TGF-β1 Emax immune Assay System ELISA kit (Promega, Madison, WI, USA) according to the manufacturer's instructions. Samples were acidified using 1 N HCl to a pH of 3.0 for 15–20 min, followed by neutralization with 1 N NaOH before they were subjected to ELISA.

2.9. Real-time RT-PCR

Total RNA isolation and real-time RT-PCR were performed as described previously [18]. Briefly, total RNA was extracted using the RNeasy micro kit (Qiagen, Valencia, CA) according to the manufacturer's protocols. RNA (0.5 μg) was reverse transcribed to

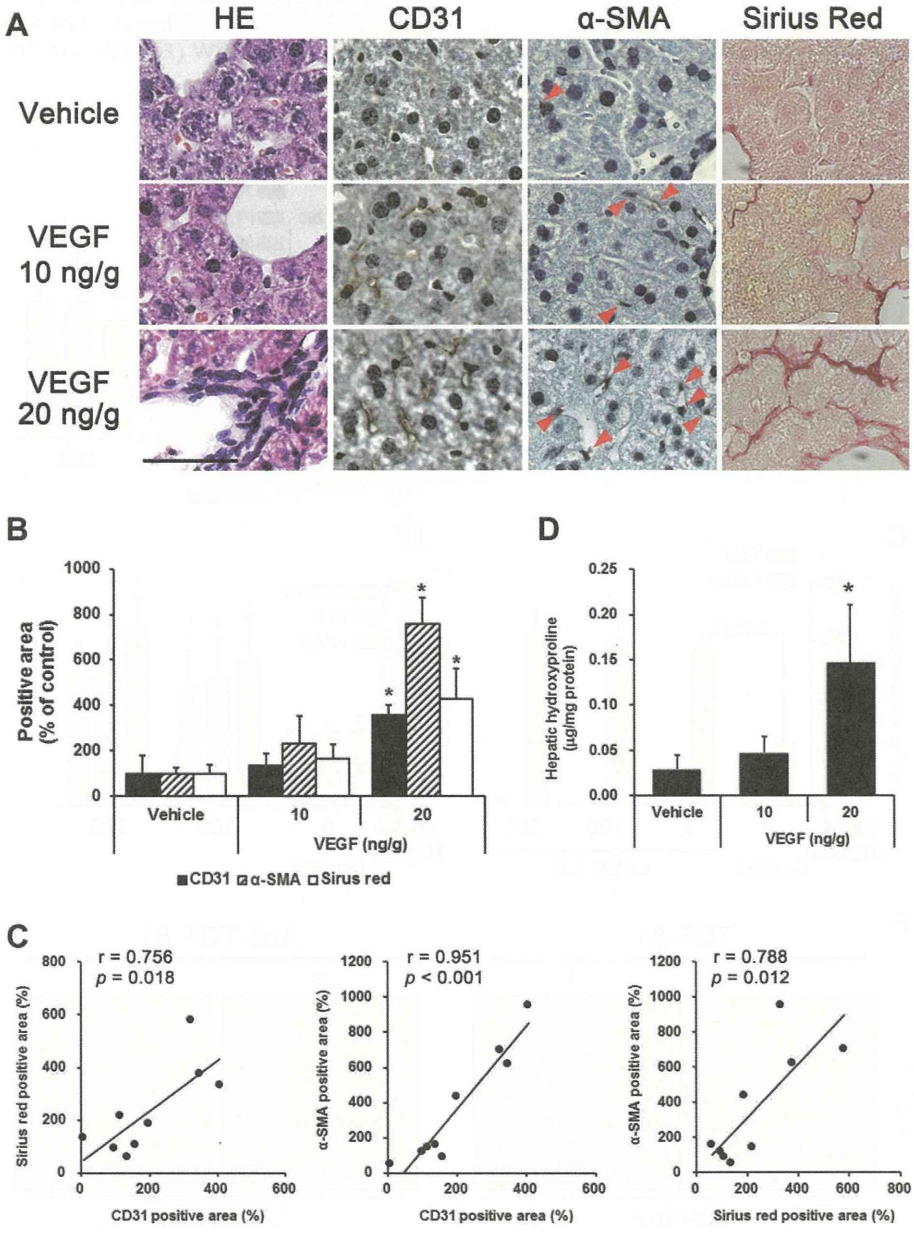

Fig. 1. VEGF simultaneously induced angiogenesis and fibrogenesis in the liver. Saline (100 μl/mouse/day) with or without recombinant VEGF at the indicated doses was injected into the tail vein of three 10-week-old C57BL/6 mice for 10 days. Their livers were removed after the animals were euthanized. (A) Liver tissue sections were prepared and stained with HE, antibodies for CD31 and α-SMA, and Sirius red, as described in the Section 2. Scale bar is 50 μm. Red arrow heads represent α-SMA positive cells. (B) CD31, α-SMA and Sirius red-positive areas (%) were quantitated and plotted as the means ± SD in the bar graphs ($n = 3$). (C) The correlation between CD31 and Sirius red-positive area (left panel), CD31 and α-SMA-positive area (middle panel), and Sirius red- and α-SMA-positive area (right panel). (D) The liver HDP levels were measured as described in the Section 2. *$p < 0.05$ compared with vehicle-treated mice.

cDNA using the PrimeScript® RT Master Mix (Takara Bio Inc., Shiga, Japan). mRNA expression levels were determined using real-time PCR. Real-time PCR was performed with the Thermal Cycler Dice® Real Time System using the SsoAdvanced™ SYBR® Green Supermix (Bio-Rad Laboratories, Hercules, CA) and normalized to 18S rRNA expression. The primer sequences used were as follows: mouse TGF-β1 forward: 5′-GCA ACA ATT CCT GGC GTT ACC-3′, reverse: 5′-CCC TGT ATT CCG TCT CCT TGG T-3′; mouse PLK forward: 5′-GAC CAG AGT ACC GGA AGA AG-3′, reverse: 5′-ACC TAT CTC CGA AAG CGC AC-3′; mouse uPAR forward: 5′-GCC GCT ATC CTA CAG AGC AC-3′, reverse: 5′-GCT ATG GAA ACC TGC TGT GCC-3′; and 18S rRNA forward: 5′-GTA ACC CGT TGA ACC CCA TT-3′, reverse: 5′-CCA TCC AAT CGG TAG TAG CG-3′.

2.10. Statistics

Statistical analyses were performed using one-way analysis of variance, followed by the Dunnett's or Tukey's post hoc tests. A two-tailed Student's *t*-test was used to evaluate the differences between the two groups.

3. Results

3.1. Simultaneous induction of hepatic angiogenesis and fibrogenesis in mice after injection of VEGF

VEGF administration to mice dose-dependently increased the number of cellular infiltrations, endothelial cells (CD31 staining, 3.6-fold at 20 ng VEGF/g of BW), and active HSCs (α-SMA staining, red arrow heads, 7.6-fold at 20 ng VEGF/g of BW), which accompanied an increase in the Sirius red-positive area (4.3-fold at 20 ng VEGF/g of BW) (Fig. 1A and B). Significant correlations were observed among the positive areas of CD31, α-SMA, and Sirius red (Fig. 1C). The hepatic hydroxyproline levels also increased 5-fold at 20 ng VEGF/g of BW (Fig. 1D) and 10-fold at 30 ng VEGF/g of BW (data not shown).

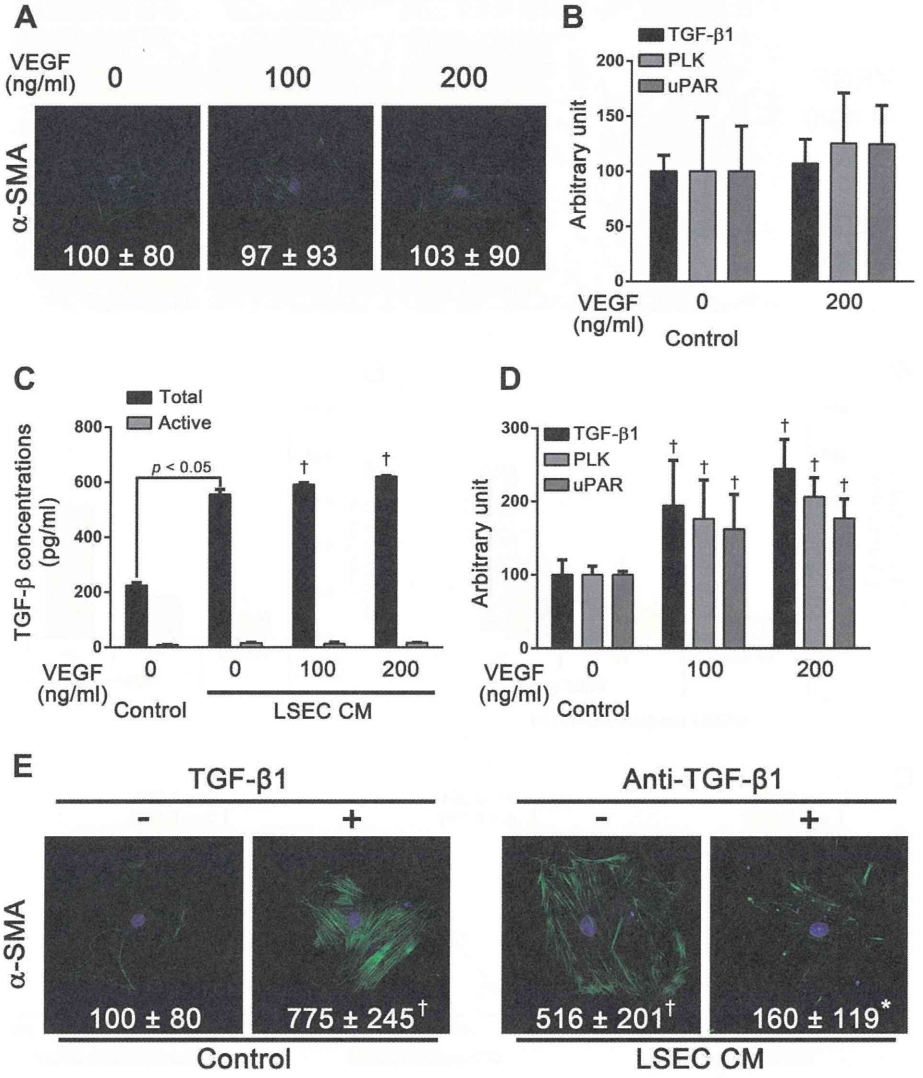

Fig. 2. LSEC CM enhanced HSC activation via TGF-β. Primary HSCs were incubated with 2% FBS DMEM in the presence or absence of the indicated concentrations of recombinant VEGF (A and B), TGF-β1 (100 pg/ml), and LSEC CM in the presence or absence of neutralizing anti-TGF-β1 (2.5 μg/ml) (E) for 5 days. Primary LSECs were incubated with 2% FBS DMEM/F12 in the presence or absence of the indicated concentrations of recombinant VEGF for 24 h (C and D). (A and E) Cells were fixed and stained with α-SMA as described in the Section 2. The relative fluorescence intensities (% of untreated control cells) are shown as the mean ± SD. (B and D) The mRNA expression levels of TGF-β1, PLK, and uPAR were measured using real-time RT-PCR as described in the Section 2. (C) Total/active TGF-β1 levels in the media were measured as described in the Section 2. †$p < 0.05$ compared with untreated control cells, *$p < 0.05$ compared with LSEC CM-treated control cells.